3-D seismic images of an extensive igneous sill in the lower crust

T. Wrona[1,2]*, C. Magee[3,4], H. Fossen[5], R. L. Gawthorpe[1], R. E. Bell[3], C. A-L. Jackson[3] & J. I. Faleide[6]

[1]Department of Earth Science, University of Bergen, Allgaten 41, N-5007 Bergen, Norway.
[2]Norwegian Academy of Science & Letters, Drammensveien 78, 0271 Oslo, Norway.
[3]Basins Research Group (BRG), Department of Earth Science and Engineering, Imperial College, Prince Consort Road, London, SW7 2BP, UK.
[4]School of Earth and Environment, University of Leeds, Leeds, LS2 9JT, UK
[5]Museum of Natural History, University of Bergen, Allgaten 41, N-5007 Bergen, Norway.
[6]Department of Geosciences, University of Oslo, P.O. Box 1047 Blindern, N-0316 Oslo, Norway.

*thilo.wrona@uib.no

Abstract

When continents rift, magmatism can produce large volumes of melt that migrate upwards from deep below the Earths surface. To understand how magmatism impacts rifting, it is critical to understand how much melt is generated and how it transits the crust. Estimating melt volumes and pathways is difficult, however, particularly in the lower crust where the resolution of geophysical techniques is limited. New broadband seismic reflection data allow us to image the three-dimensional (3-D) geometry of magma crystallized in the lower crust (17.5-22 km depth) of the northern North Sea, in an area previously considered a magma-poor rift. The sub-horizontal igneous sill is ~97 km long (N-S), ~62 km wide (E-W), and 180±40 m thick. We estimate that 472±161 km^3 of magma was emplaced within this intrusion, suggesting that the northern North Sea contains more igneous intrusions than previously thought. The significant areal extent of the intrusion (~2700 km^2), as well as presence of intrusive steps, indicate sills can facilitate widespread lateral magma transport in the lower crust.

Keywords: Magma, lower crust, igneous sill, 3-D seismic reflection data, North Sea

1 Introduction

The style of continental rifting critically depends on the strength of the lower crust (e.g., Huismans and Beaumont, 2011), which may be changed by magmatic processes including melting, magma migration, and crystallization. To study the effects of magmatism on rifting, we need to understand the distribution and volume of magma emplaced in the crust in three dimensions (e.g. White et al., 2008). Whilst the current paradigm for magma plumbing system structure broadly advocates that vertically stacked sills accumulate and store melt within the lower crust (e.g. Annen et al., 2005; Annen et al., 2015; Cashman et al., 2017; Edmonds et al., 2019), the lateral extent of these intrusion networks remains poorly understood. Three-dimensional seismic reflection data showing acoustic images of the subsurface have revolutionized our understanding of magma plumbing systems in the upper crust (e.g., Trude et al., 2003; Planke et al., 2005). In contrast, in the lower crust, seismic studies have long been limited by data coverage and resolution, providing an incomplete picture of the geometry and distribution of lower crustal intrusions (e.g., Cartwright and Hansen, 2006; Abdelmalak et al., 2017).

Using one of the largest 3-D seismic reflection surveys ever acquired (courtesy of CGG), covering 35,410 km^2 of the northern North Sea rift and imaging down to depths of 22 km (see Supplementary Texts 1 and 2), we are able to analyze lower crustal structures at a resolution of a few tens of meters over thousands of square kilometers. This analysis allows us to critically examine and develop hypotheses for the origin of a lower crustal reflection (LCR), which has previously been identified in sparse 2-D seismic profiles (Christiansson et al., 2000; Fichler et al., 2011) but which we here are able to map in 3-D. Combining a series of detailed seismic (e.g. amplitude, polarity, continuity) and geometric observations (e.g. lobes, saucers, intrusive steps), we conclude that the LCR originates from an extensive igneous sill (±2700 km^2), which previously stored significant volumes of magma (472±161 km^3) deep in the lower crust (17.5-22 km).

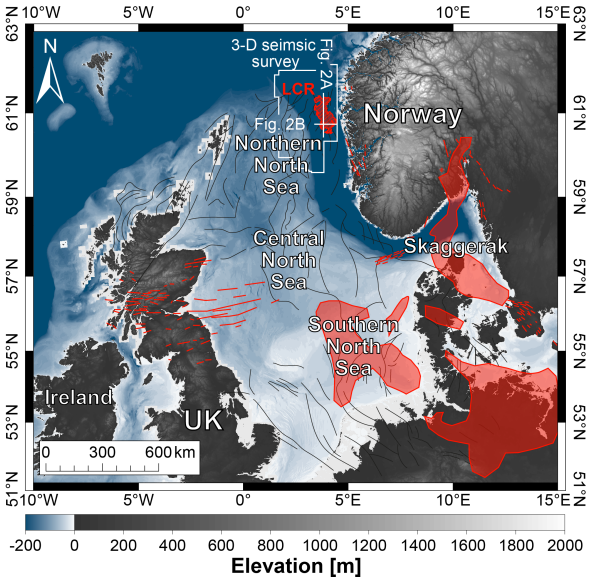

Figure 1: Location map of the North Sea showing the area covered by the 3-D seismic survey (courtesy of CGG) with LCR (white outline), magmatic dikes (red lines), tectonic faults (black lines) and volcanic rocks (red polygons) emplaced between the Late Carboniferous (∼300 Ma) and the Late Triassic (∼220 Ma) as part of the Skagerrak-centered Large Igneous Province (Fossen and Dunlap, 1999; Bingen and Solli, 2009; Fazlikhani et al., 2017). Offshore the distribution of volcanic rocks is constrained by well and seismic data (Heeremans and Faleide, 2004; Torsvik et al., 2008; Phillips et al., 2017). Topography and bathymetry are from ESRIs World Elevation Service (Weatherall et al., 2015).

2 Geological setting

The study area is located in the northern North Sea (Fig. 1), where continental crust consists of 1030 km thick crystalline basement overlain by up to 12 km of sedimentary strata deposited during, after, and possibly even before periods of Late Permian-Early Triassic and Middle Jurassic-Early Cretaceous rifting (e.g., Bell et al., 2014; Maystrenko et al., 2017). The crystalline basement formed by terrain accretion during the Sveconorwegian (1140-900 Ma) and Caledonian (460-400 Ma) orogenies (Bingen et al., 2008). During the Caledonian orogeny, subduction of continental crust subjected some of these basement rocks to high-

and ultra-high pressure metamorphic conditions sufficient for partial eclogitization (Austrheim, 1987). A lower crustal reflection (LCR) identified in older two-dimensional (2-D) seismic reflection data imaging our study area is characterized by a high-amplitude and positive polarity, and has previously been suggested to mark the top of a km-thick volume of eclogitized rocks (Christiansson et al., 2000). In contrast, based on 2-D gravity and magnetic modelling, Fichler et al. (2011) infer that the LCR defines the boundary between overlying continental crust and an underlying, high magnetic susceptibility, serpentinized mantle wedge. Testing these existing hypotheses for the origin of the LCR in the context of the geodynamic evolution of the northern North Sea using 3-D seismic reflection data is the focus of this study.

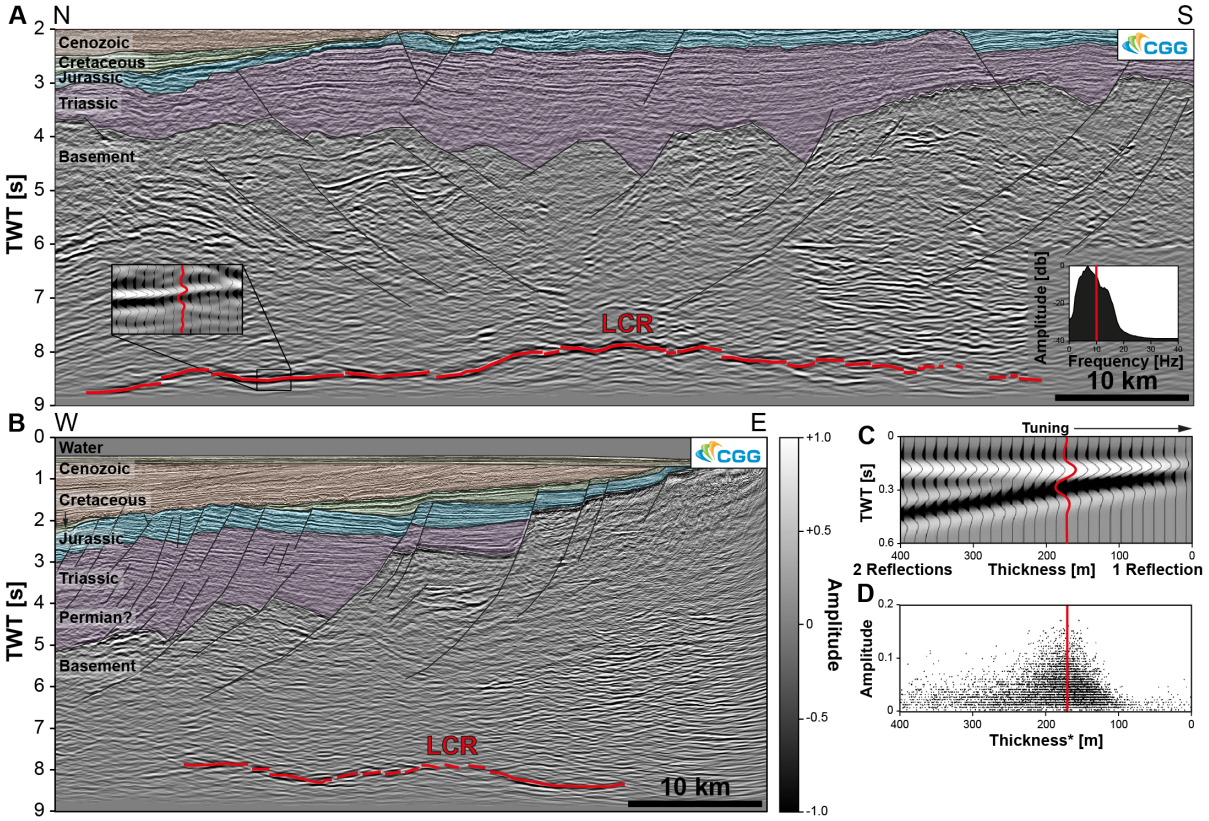

Figure 2: **A:** North-south seismic sections showing the lower crustal reflection (LCR) with close-up of seismic trace indicating peak-trough- wavelet similar to tuning wedge (**C**) and with frequency amplitude spectrum showing dominant frequencies of 10±2 Hz around the LCR. **B:** East-west seismic section. **C:** Tuning wedge model based on acoustic impedance increase with depth. **D:** Thickness versus amplitude cross-plot of the LCR with *thicknesses calculated from time difference between top and bottom reflection using an interval velocity of 7 km/s (Rosso, 2007). Note consistency of thickness estimates (180±40 m) between **C** and **D**. Seismic data courtesy of CGG.

3 Observations

The LCR appears as a high-amplitude, positive polarity seismic reflection in the lower crust at depths of 17.522 km depth (Figs. 2, 3; Supplementary Fig. 1), and can be mapped continuously over ∼2700 km^2 (Fig. 4, Supplementary Fig. 2). The LCR is ∼97 km long (N-S) and ∼62 km wide (E-W), consisting of several irregular lobes that laterally extend up to ∼20 km outwards from its center (Fig. 3B, 4, Supplementary Animation 1). These irregular lobes consist of several smaller, laterally connected saucer geometries (i.e. a flat inner surface that passes laterally into an inclined limb) (Figs. 3B; 4).

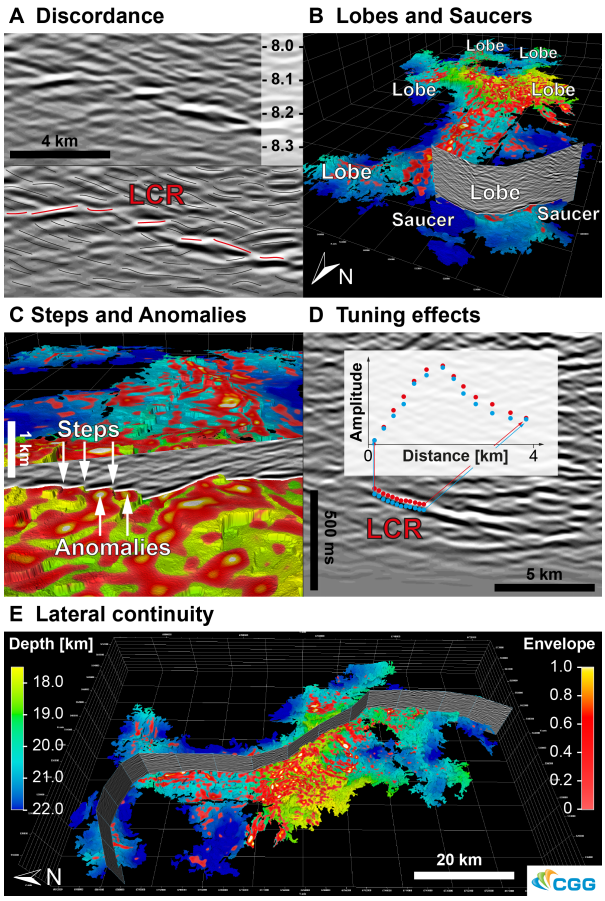

Figure 3: Seismic features of the LCR indicative of an igneous intrusion. **A:** Comparison between uninterpreted and interpreted seismic section showing discordance between the LCR and host strata (cf. Cartwright and Hansen, 2006; Magee et al., 2016), **B:** Lobe geometries extending outwards from the LCR (cf. Smallwood and Maresh, 2002; Magee et al., 2016) and saucer geometries showing a flat inner sill that passes laterally into an inclined limb (cf. Polteau et al., 2008; Haug et al., 2018; Infante-Paez and Marfurt, 2018; Schmiedel et al., 2019). **C:** Intrusive steps, i.e. i.e. laterally-elongated vertical steps (cf. Hansen et al., 2004; Magee et al., 2016; McBride et al., 2018) with elongated amplitude anomalies (cf. Smallwood and Maresh, 2002). **D:** Tuning effects due to the interference of waves originating from the top and base of a thin body, **E:** Lateral continuity of the LCR over a large area (~2700 km^2) (cf. Magee et al., 2016) shown by 3-D surface and 2-D seismic section (see Supp. Fig. 2). Surfaces on B,C and E show the depth of the LCR (in kilometer below the seafloor) overlain by the amplitude envelope extracted along the surface. Seismic data courtesy of CGG.

These saucers are also the deepest part of the LCR, extending down to a depth of 22 km, whereas the central part of the LCR is much shallower (17.5 km). The center of the LCR displays a series of elongated, 100300 m high vertical steps that cross-cut discontinuous, medium- to low-amplitude, background reflections (Figs. 3A, 4). We observe several elongate high-amplitude anomalies aligned along these vertical steps in the horizontal plane (Figs. 3C, 4).

In general, the LCR shows: (1) high amplitudes, (2) a peak-trough wavelet, and (3) approximately equal peak and trough amplitudes, features that are typical of tuning effects (e.g., Widess, 1973; Robertson and Nogami, 1984; Sheriff and Geldart, 1995) (Figs. 2, 3D). Tuning occurs when seismic waves originating from the top and base of a thin body interfere on their return to the surface (e.g., Brown, 2011). We can estimate the thickness of a body where constructive interference from top and base produces a single tuned response, rather than two separate seismic reflections. Based on observed dominant frequencies of 10±2 Hz (Fig. 2A) and seismic velocities of 6.9±0.1 km/s for these basement rocks, derived from a recent wide-angle 2-D seismic survey (Rosso (2007), we estimate that the LCR originates from a 180±4 m thick body (Fig. 2C); this tuning thickness is consistent with an independent estimate based on an amplitude vs. thickness cross-plot (Connolly, 2005; Francis, 2015) (Fig. 2D) (see Appendix: Tuning thickness).

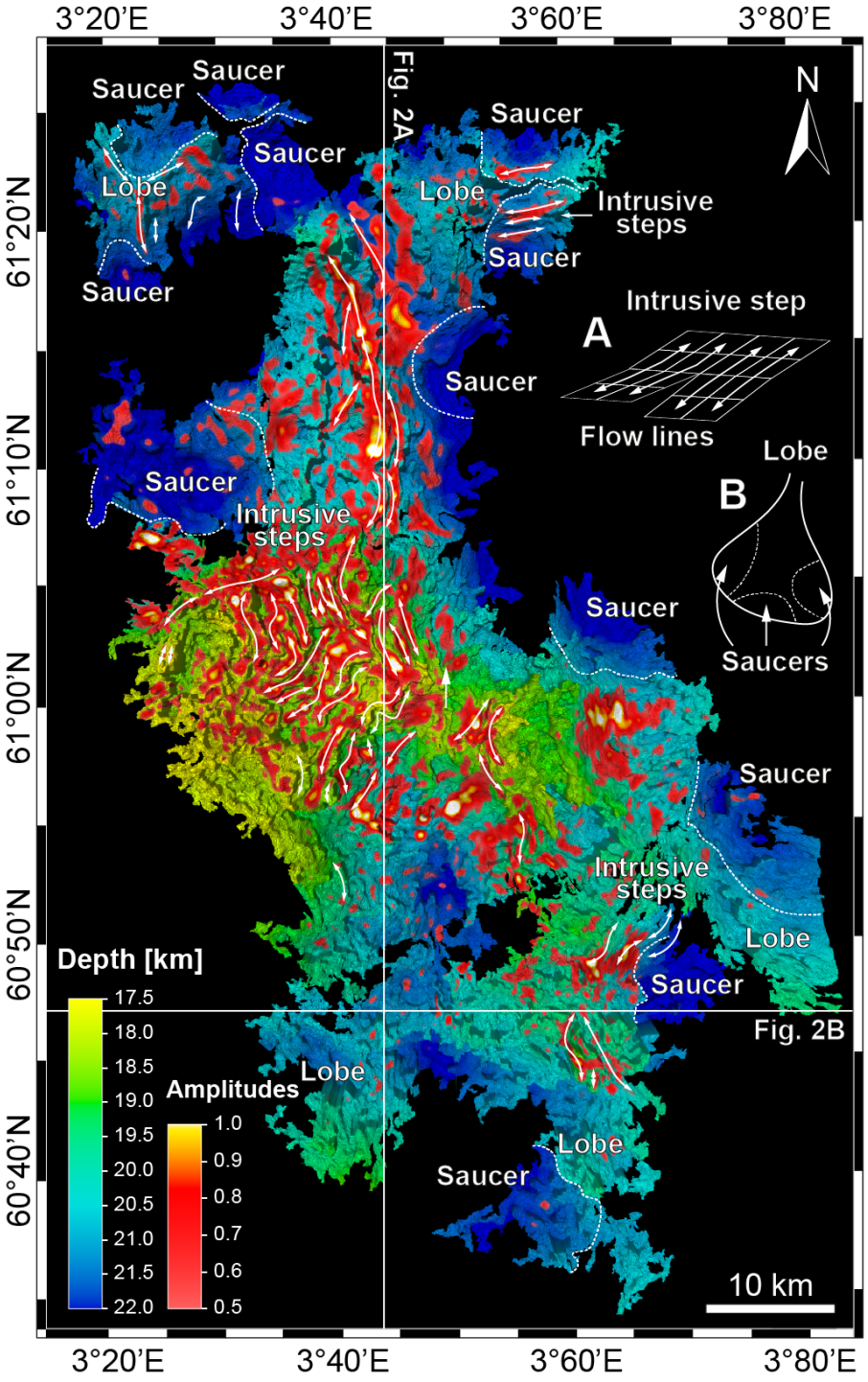

Figure 4: 3-D geometry of lower crustal reflection (LCR) originating from an igneous sill. Evidence for the LCR being an igneous intrusion includes: (1) significant lateral continuity (~2700 km^2) (cf. Magee et al., 2016); (2) irregular lobes extending outwards (cf. Smallwood and Maresh, 2002; Magee et al., 2016), (3) saucer-shape geometries forming parts of these lobes (see B) (cf. Polteau et al., 2008; Haug et al., 2018; Infante-Paez and Marfurt, 2018; Schmiedel et al., 2019); (4) intrusive steps (cf. Hansen et al., 2004; Magee et al., 2016; McBride et al., 2018) and (5) elongated amplitude anomalies (cf. Smallwood and Maresh, 2002). Magma flow lines are drawn from elongated amplitude anomalies perpendicular to intrusive steps (see A). Depth conversion is based on shallow (0-5 km) checkshot and deep (5-22 km) seismic data (Rosso, 2007; Bell et al., 2014). A 3-D animation of the surface can be found in the supplementary material. Seismic data courtesy of CGG.

4 Discussion

We observe that the LCR shows typical effects of tuning (e.g. equal peak and trough amplitudes; Fig. 3D), which implies that it originates from a thin layer rather than the top of a several km-thick rock volume (cf. Christiansson et al., 2000; Fichler et al., 2011). Furthermore, the suggested eclogitization (Christiansson et al., 2000) and serpentinization origins for the LCR (Fichler et al., 2011) are at odds with observed velocities and the polarity of the LCR. For example, whilst eclogitization was initially postulated based on inferred seismic velocities of >8 km/s in the region of the LCR (Christiansson et al., 2000), recent wide-angle 2-D reflection and refraction data reveal normal velocities of 6.9±0.1 km/s (Rosso, 2007) (see Appendix for more details). In contrast, serpentinization reduces seismic velocities (Christensen, 2004), which would result in a downward decrease in acoustic impedance and a negative polarity reflection, rather than the normal polarity we observe for the LCR (e.g. Figs. 2, 3).

After examining previous interpretations of the LCR, we now discuss other explanations for lower crustal reflections. Reflections from highly strained rocks within a shear zone could explain the tuning effects, but shear zones are usually several kilometers thick in the lower crust and typically imaged as multiple, subparallel seismic reflections (Clerc et al., 2015; Fazlikhani et al., 2017). As such, it is difficult to explain the isolated, sub-horizontal reflection we observe (e.g. Fig. 2) in terms of a ductile, lower-crustal shear zone. Instead, we observe that the LCR shows the characteristic features of igneous intrusions observed in the field, seismic reflection data, and numerical models. First, the LCR cross-cuts numerous inclined, discontinuous background reflections that originate from the host stratigraphy (Fig. 3A). Discordance between igneous intrusions and the host stratigraphy is commonly observed in seismic images from sedimentary basins and develops when magma cross-cuts existing strata without offsetting it (e.g. Cartwright and Hansen, 2006; Magee et al., 2016; Eide et al., 2017). Second, the LCR shows irregular lobes extending outward from its central axis (Fig. 3B). Similar lobes are commonly observed in igneous sills (i.e. tabular sheet intrusions) imaged by 3-D seismic reflection data, as well as those observed in field exposures, and form by incremental emplacement of discrete magma injections (e.g. Smallwood and Maresh, 2002; Schofield et al., 2012a; Magee et al., 2016). Third, these lobes are themselves comprised of a series of saucers consisting of a flat inner surface that passes laterally into an inclined limb (Fig. 3B). Numerous sills observed in the field, seismic reflection data, and produced in numerical and analogue models display saucer-shaped morphologies, formed when a relatively flat sill develops transgressive inclined limbs in response to stress perturbations and/or host rock deformation at its lateral tips (e.g. Malthe-Srenssen et al., 2004; Polteau et al., 2008; Haug et al., 2018; Schmiedel et al., 2019). Fourth, the LCR contains several elongated, linear, vertical steps (Fig. 3C), which appear similar to intrusive steps formed during sheet propagation and are a record of magma flow (e.g., Hansen et al., 2004; Magee et al., 2016; Magee et al., 2018; McBride et al., 2018). Fifth, the LCR displays laterally-elongated amplitude anomalies (Fig. 3C), which likely relate to subtle, local variations in intrusion thickness and may correspond to magma flow channels (cf. Holness and Humphreys, 2003). Sixth, the tuning effects displayed by the LCR are indicative of reflections emanating from a thin body (Figs. 2C; 3D), consistent with the seismic expression of relatively thin sills observed in real and synthetic seismic reflection data (¡300 m; Magee et al., 2016). Seventh, the LCR is continuous over a large area (∼2700 km^2) (Fig. 3E), a common feature of sills, which can extend over several hundreds of kilometers (e.g. Magee et al., 2016). The combination of these observations supports our interpretation that the LCR originates from an igneous sill.

5 Implications

We estimate a magma volume of 472±161 km^3 for the LCR by multiplying the surface area (∼2700 km^2) with the inferred tuning thickness (180±40 m). Whilst the LCR intrusion is less voluminous than the largest exposed or

seismically imaged sills (e.g. sills in the Ferrar sill-complex or Antractica of up to 105 km3), it is still more extensive than most sills in the Karoo or Franklin sill complexes (Cruden et al., 2017). The LCR intrusion volume is of the same order of magnitude as layered mafic intrusions emplaced in sedimentary rocks (see Fig. 1b in Cruden et al., 2017) as well as stacked lower crustal intrusions mapped in 2-D seismic reflection data from the North Atlantic margin (540-600 km^3; White et al., 2008). Constraining the composition of this intrusion is not possible given the uncertainty in measured velocity measurements (6.9±0.1 km/s; Rosso, 2007) and the insensitivity of seismic velocities to compositional variations in igneous rocks (Behn and Kelemen, 2003; Bartetzko et al., 2005). In addition to our volume estimates, we constrain magma flow patterns within the LCR using intrusive steps (Fig. 3D) and amplitude anomalies (Fig. 3E). Intrusive steps form because propagating sheets are commonly segmented, with individual segments intruding at slightly different structural levels (e.g. Schofield et al., 2012b; Magee et al., 2018). As magma intrusion continues and the segments inflate, they coalesce to form a through-going sill that contains vertical steps marking segment boundaries, with the long axes of steps and segments reflecting the initial sheet propagation direction (e.g. Schofield et al., 2012b; Magee et al., 2018). This process results in thickness variations, which translate into amplitude anomalies due to tuning effects (Magee et al., 2015). We observe these elongated amplitude anomalies on the LCR in map view (Fig.). The presence of up to 20 km long steps and amplitude anomalies, which may represent magma channels within the LCR, implies that emplacement occurred primarily through lateral flow, rather than by amalgamation of many small sills fed by dykes. Whilst magma plumbing systems are typically depicted as dyke-dominated, with sills forming vertically stacked storage reservoirs in the lower or upper crust (e.g. Annen et al., 2005; Annen et al., 2015; Cashman et al., 2017; Edmonds et al., 2019), our observations highlight significant horizontal transport in the lower crust.

6 Conclusions

This study reveals a lower crustal igneous intrusion in a continental rift (northern North Sea), which has long been considered magma-poor. This sill is ∼97 km long in north-south and ∼62 km wide in east-west direction showing evidence for significant lateral transport (up to 20 km) of large volumes of magma (472±161 km^3). This study shows how advanced 3-D seismic imaging can help us understand magmatic processes occurring deep within the crust.

Acknowledgements

Financial support for this project was provided by The Norwegian Academy of Science and Letters and The University of Bergen. We thank CGG, in particular Stein Åsheim, for the permission to use and publish this data. Furthermore, we thank Schlumberger for providing the software Petrel 2017 and Leo Zijerveld for IT support.

References

Abdelmalak, M. M., Faleide, J. I., Planke, S., Gernigon, L., Zastrozhnov, D., Shephard, G. E., and Myklebust, R. (2017). The treflection and the deep crustal structure of the vring margin, offshore midnorway. *Tectonics*, 36(11):2497–2523.

Annen, C., Blundy, J., and Sparks, R. (2005). The genesis of intermediate and silicic magmas in deep crustal hot zones. *Journal of Petrology*, 47(3):505–539.

Annen, C., Blundy, J. D., Leuthold, J., and Sparks, R. S. J. (2015). Construction and evolution of igneous bodies: Towards an integrated perspective of crustal magmatism. *Lithos*, 230:206–221.

Austrheim, H. (1987). Eclogitization of lower crustal granulites by fluid migration through shear zones. *Earth and Planetary Science Letters*, 81(2-3):221–232.

Bartetzko, A., Delius, H., and Pechnig, R. (2005). Effect of compositional and structural variations on log responses of igneous and metamorphic rocks. i: mafic rocks. *Geological Society, London, Special Publications*, 240(1):255–278.

Behn, M. D. and Kelemen, P. B. (2003). Relationship between seismic p-wave velocity and the composition of anhydrous igneous and meta-igneous rocks. *Geochemistry Geophysics Geosystems*, 4(5).

Bell, R. E., Jackson, C. A. L., Whipp, P. S., and Clements, B. (2014). Strain migration during multiphase extension: Observations from the northern north sea. *Tectonics*, 33(10):1936–1963.

Bingen, B., Nordgulen, O., and Viola, G. (2008). A four-phase model for the sveconorwegian orogeny, sw scandinavia. *Norwegian Journal of Geology*, 88(1):43–72.

Bingen, B. and Solli, A. (2009). Geochronology of magmatism in the caledonian and sveconorwegian belts of baltica: synopsis for detrital zircon provenance studies. *Norwegian Journal of Geology*, 89(4):267–290.

Brown, A. R. (2011). *Interpretation of Three-Dimensional Seismic Data*. The American Association of Petroleum Geologists and the Society of Exploration Geophysicists.

Cartwright, J. and Hansen, D. M. (2006). Magma transport through the crust via interconnected sill complexes. *Geology*, 34(11):929–932.

Cashman, K. V., Sparks, R. S., and Blundy, J. D. (2017). Vertically extensive and unstable magmatic systems: A unified view of igneous processes. *Science*, 355(6331):eaag3055.

Christensen, N. I. (2004). Serpentinites, peridotites, and seismology. *International Geology Review*, 46(9):795–816.

Christiansson, P., Faleide, J. I., and Berge, A. M. (2000). Crustal structure in the northern north sea: an integrated geophysical study. *Geological Society, London, Special Publications*, 167(1):15–40.

Clerc, C., Jolivet, L., and Ringenbach, J. C. (2015). Ductile extensional shear zones in the lower crust of a passive margin. *Earth and Planetary Science Letters*, 431:1–7.

Connolly, P. (2005). Net pay estimation from seismic attributes. In *67th EAGE Conference & Exhibition*.

Cruden, A., McCaffrey, K., and Bunger, A. (2017). *Geometric scaling of tabular igneous intrusions: Implications for emplacement and growth*, pages 11–38. Springer.

Edmonds, M., Cashman, K. V., Holness, M., and Jackson, M. (2019). Architecture and dynamics of magma reservoirs.

Eide, C. H., Schofield, N., Lecomte, I., Buckley, S. J., and Howell, J. A. (2017). Seismic interpretation of sill complexes in sedimentary basins: implications for the sub-sill imaging problem. *Journal of the Geological Society*, pages jgs2017–096.

Fazlikhani, H., Fossen, H., Gawthorpe, R. L., Faleide, J. I., and Bell, R. E. (2017). Basement structure and its influence on the structural configuration of the northern north sea rift. *Tectonics*, 36(6):1151–1177.

Fichler, C., Odinsen, T., Rueslltten, H., Olesen, O., Vindstad, J. E., and Wienecke, S. (2011). Crustal inhomogeneities in the northern north sea from potential field modeling: Inherited structure and serpentinites? *Tectonophysics*, 510(1-2):172–185.

Fossen, H. and Dunlap, W. J. (1999). On the age and tectonic significance of permo-triassic dikes in the bergen-sunnhordland region, southwestern norway. *Norsk Geologisk Tidsskrift*, 79(3):169–177.

Francis, A. (2015). A simple guide to seismic amplitudes and detuning. *GeoExPro*, 12(5).

Hansen, D. M., Cartwright, J. A., and Thomas, D. (2004). 3d seismic analysis of the geometry of igneous sills and sill junction relationships. *Geological Society, London, Memoirs*, 29(1):199–208.

Haug, ., Galland, O., Souloumiac, P., Souche, A., Guldstrand, F., Schmiedel, T., and Maillot, B. (2018). Shear versus tensile failure mechanisms induced by sill intrusions: Implications for emplacement of conical and saucershaped intrusions. *Journal of Geophysical Research: Solid Earth*, 123(5):3430–3449.

Heeremans, M. and Faleide, J. I. (2004). Late carboniferous-permian tectonics and magmatic activity in the skagerrak, kattegat and the north sea. *Geological Society, London, Special Publications*, 223(1):157–176.

Holness, M. B. and Humphreys, M. C. S. (2003). The traigh bhan na sgurra sill, isle of mull: Flow localization in a major magma conduit. *Journal of Petrology*, 44(11):1961–1976.

Huismans, R. and Beaumont, C. (2011). Depth-dependent extension, two-stage breakup and cratonic underplating at rifted margins. *Nature*, 473(7345):74–8.

Infante-Paez, L. and Marfurt, K. J. (2018). In-context interpretation: Avoiding pitfalls in misidentification of igneous bodies in seismic data. *Interpretation-a Journal of Subsurface Characterization*, 6(4):Sl29–Sl42.

Magee, C., Maharaj, S. M., Wrona, T., and Jackson, C. A. L. (2015). Controls on the expression of igneous intrusions in seismic reflection data. *Geosphere*, 11(4):1024–1041.

Magee, C., Muirhead, J., Schofield, N., Walker, R. J., Galland, O., Holford, S., Spacapan, J., Jackson, C. A., and McCarthy, W. (2018). Structural signatures of igneous sheet intrusion propagation. *Journal of Structural Geology*.

Magee, C., Muirhead, J. D., Karvelas, A., Holford, S. P., Jackson, C. A. L., Bastow, I. D., Schofield, N., Stevenson, C. T. E., McLean, C., McCarthy, W., and Shtukert, O. (2016). Lateral magma flow in mafic sill complexes. *Geosphere*, 12(3):809–841.

Malthe-Srenssen, A., Planke, S., Svensen, H., Jamtveit, B., Breitkreuz, C., and Petford, N. (2004). Formation of saucer-shaped sills. *Physical geology of high-level magmatic systems. Geological Society, London, Special Publications*, 234:215–227.

Maystrenko, Y. P., Olesen, O., Ebbing, J., and Nasuti, A. (2017). Deep structure of the northern north sea and southwestern norway based on 3d density and magnetic modelling. *Norwegian Journal of Geology*, 97(3):169–210.

McBride, J. H., Keach, R. W., Leetaru, H. E., and Smith, K. M. (2018). Visualizing precambrian basement tectonics beneath a carbon capture and storage site, illinois basin. *Interpretation-a Journal of Subsurface Characterization*, 6(2):T257–T270.

Odinsen, T., Christiansson, P., Gabrielsen, R. H., Faleide, J. I., and Berge, A. M. (2000). The geometries and deep structure of the northern north sea rift system. *Geological Society, London, Special Publications*, 167(1):41–57.

Planke, S., Rasmussen, T., Rey, S. S., and Myklebust, R. (2005). Seismic characteristics and distribution of volcanic intrusions and hydrothermal vent complexes in the vring and mre basins. *Geological Society, London, Petroleum Geology Conference series*, 6(1):833–844.

Polteau, S., Mazzini, A., Galland, O., Planke, S., and Malthe-Sorenssen, A. (2008). Saucer-shaped intrusions: Occurrences, emplacement and implications. *Earth and Planetary Science Letters*, 266(1-2):195–204.

Robertson, J. D. and Nogami, H. H. (1984). Complex seismic trace analysis of thin beds. *Geophysics*, 49(4):344–352.

Rosso, A. (2007). *Deep crustal geometry: An integrated geophysical study of an exhumed eclogite terrain, Bergen Area, Southwest Norway.* Thesis, University of Wyoming.

Schmiedel, T., Galland, O., Haug, O. T., Dumazer, G., and Breitkreuz, C. (2019). Coulomb failure of earth's brittle crust controls growth, emplacement and shapes of igneous sills, saucer-shaped sills and laccoliths. *Earth and Planetary Science Letters*, 510:161–172.

Schofield, N., Heaton, L., Holford, S. P., Archer, S. G., Jackson, C. A.-L., and Jolley, D. W. (2012a). Seismic imaging of broken bridges: linking seismic to outcrop-scale investigations of intrusive magma lobes. *Journal of the Geological Society*, 169(4):421–426.

Schofield, N. J., Brown, D. J., Magee, C., and Stevenson, C. T. (2012b). Sill morphology and comparison of brittle and non-brittle emplacement mechanisms. *Journal of the Geological Society*, 169(2):127–141.

Sheriff, R. E. and Geldart, L. P. (1995). *Exploration Seismology.* Cambridge University Press.

Smallwood, J. R. and Maresh, J. (2002). The properties, morphology and distribution of igneous sills: modelling, borehole data and 3d seismic from the faroe-shetland area. *Geological Society, London, Special Publications*, 197(1):271–306.

Torsvik, T. H., Smethurst, M. A., Burke, K., and Steinberger, B. (2008). Long term stability in deep mantle structure: Evidence from the similar to 300 ma skagerrak-centered large igneous province (the sclip). *Earth and Planetary Science Letters*, 267(3-4):444–452.

Trude, J., Cartwright, J., Davies, R. J., and Smallwood, J. (2003). New technique for dating igneous sills. *Geology*, 31(9):813–816.

Weatherall, P., Marks, K. M., Jakobsson, M., Schmitt, T., Tani, S., Arndt, J. E., Rovere, M., Chayes, D., Ferrini, V., and Wigley, R. (2015). A new digital bathymetric model of the world's oceans. *Earth and Space Science*, 2(8):331–345.

White, R. S., Smith, L. K., Roberts, A. W., Christie, P. A., Kusznir, N. J., i, S. T., Roberts, A. M., Healy, D., Spitzer, R., Chappell, A., Eccles, J. D., Fletcher, R., Hurst, N., Lunnon, Z., Parkin, C. J., and Tymms, V. J. (2008). Lower-crustal intrusion on the north atlantic continental margin. *Nature*, 452(7186):460–4.

Widess, M. B. (1973). How thin is a thin bed? *Geophysics*, 38(6):1176–1180.

Appendix

Seismic acquisition: Seismic acquisition The seismic data (courtesy of CGG) were acquired with a G-Gun array consisting of 3 subarrays with a source array depth of 6-9 m; a source length of 16-18 m; a shot point interval of 18.75 m; source separation of 37.5 m; a volume of 0.07456 m^3 and an air pressure of 1.379e+7 Pa. The streamer consisted of 12 up to 8 km long cables with 636 channels each; a cable separation of 75 m and group spacing of 12.5 m; depths of 7-50 m covering offsets of 150-8100 m. The data was recorded with a 2 ms sample interval; 9000 ms recording length; a low cut filter (2Hz-6db/oct) and high cut (200 Hz-370 db/oct) filter.

Seismic processing: Seismic processing The seismic data were processed in 90 steps including: divergence compensation; low cut filter (1.5 Hz, 2.5 Hz); noise attenuation (e.g. swell, direct wave); spatial anti-aliasing filter (12.5 m group interval); direct wave attenuation; source de-signature; de-spike; time-variant high cut filter; receiver motion correction and de-ghosting; FK filter; cold water and tidal statics; multiple modelling with adaptive subtraction; Tau-P mute; Radon de-multiple; far angle destriping; multiple attenuation; binning (75 m interval, 107 offset planes); acquisition hole infill; 5-D regularization; 3-D true amplitude Kirchhoff pre-stack time migration; residual move-out correction; Linear FL Radon; full offset stack with time-variant inner and out mute; acquisition footprint removal; crossline K filter; residual de-striping and dynamic Q-compensation. The seismic volume was zero phase processed with SEG normal polarity.

Lower crustal velocities: Lower crustal velocities: Christiansson et al. (2000) show 1-D velocity-depth functions derived from two-ship seismic refraction data at two locations (ESP 50, ESP 51) with different methods (slope-intercept, Herglotz-Wiecherts, t^2-x^2, Tau-p, forward model). At ESP 50, the slope intercept and Tau-p method indicate lower crustal velocities of 8 km/s. At ESP 51, the slope intercept, t^2-x^2 and forward model suggest lower crustal velocities of 8 km/s. All other methods provide no velocity estimate for the lower crust. Odinsen et al. (2000) and Fichler et al. (2011) do not derive new velocity-depth data. Rosso (2007) derives new 2-D velocity-depth data by combining reflection and refraction data recorded along two transects (8 OBS and 8 REFTEK receivers) with Transect 1 (NSDP84-1) passing the two locations (ESP 50, ESP 51) analyzed by Christiansson et al. (2000). Based on a comprehensive analysis including event picking, ray-tracing and uncertainty estimation for the entire dataset, Rosso (2007) concluded that the lower crust has velocities of 6.9±0.1 km/s.

Tuning thickness: Tuning thickness: While we have already estimated the tuning thickness (180±40 m) from the seismic velocity (6.9±0.1 km/s) and dominant frequency (10±2 Hz) of the interval of interest as a quarter of the wavelength (λ/4=v/f/4), we validate this value with a second estimate based on the amplitude versus thickness cross-plot (Fig. 2D). This estimate is based on the effect that an amplitude maximum occurs at the point of maximum constructive interference between the top and base reflection, i.e. the tuning thickness (Connolly, 2005; Francis, 2015). For this estimate, we first extract the amplitude of the top of the LCR and then calculate the thickness by multiplying the time difference between top and base of the LCR with the seismic velocity (6.9±0.1 km/s; Rosso, 2007). Cross-plotting the amplitude versus thickness reveals a maximum at a thickness of ∼180 m indicating that this tuning thickness estimate is consistent with the standard estimate based on a quarter of the wavelength (Brown, 2011).

While we have already estimated the tuning thickness (180±40 m) from the seismic velocity (6.9±0.1 km/s) and dominant frequency (10±2 Hz) of the interval of interest as a quarter of the wavelength (λ/4=v/f/4), we validate this value with a second estimate based on the amplitude versus thickness cross-plot (Fig. 2D). This estimate is based on the effect that an amplitude maximum occurs at the point of maximum constructive interference between the top and base reflection, i.e. the tuning thickness (Connolly, 2005; Francis, 2015). For

this estimate, we first extract the amplitude of the top of the LCR and then calculate the thickness by multiplying the time difference between top and base of the LCR with the seismic velocity (6.9±0.1 km/s; Rosso, 2007). Cross-plotting the amplitude versus thickness reveals a maximum at a thickness of ∼180 m indicating that this tuning thickness estimate is consistent with the standard estimate based on a quarter of the wavelength.

Supplementary Figures

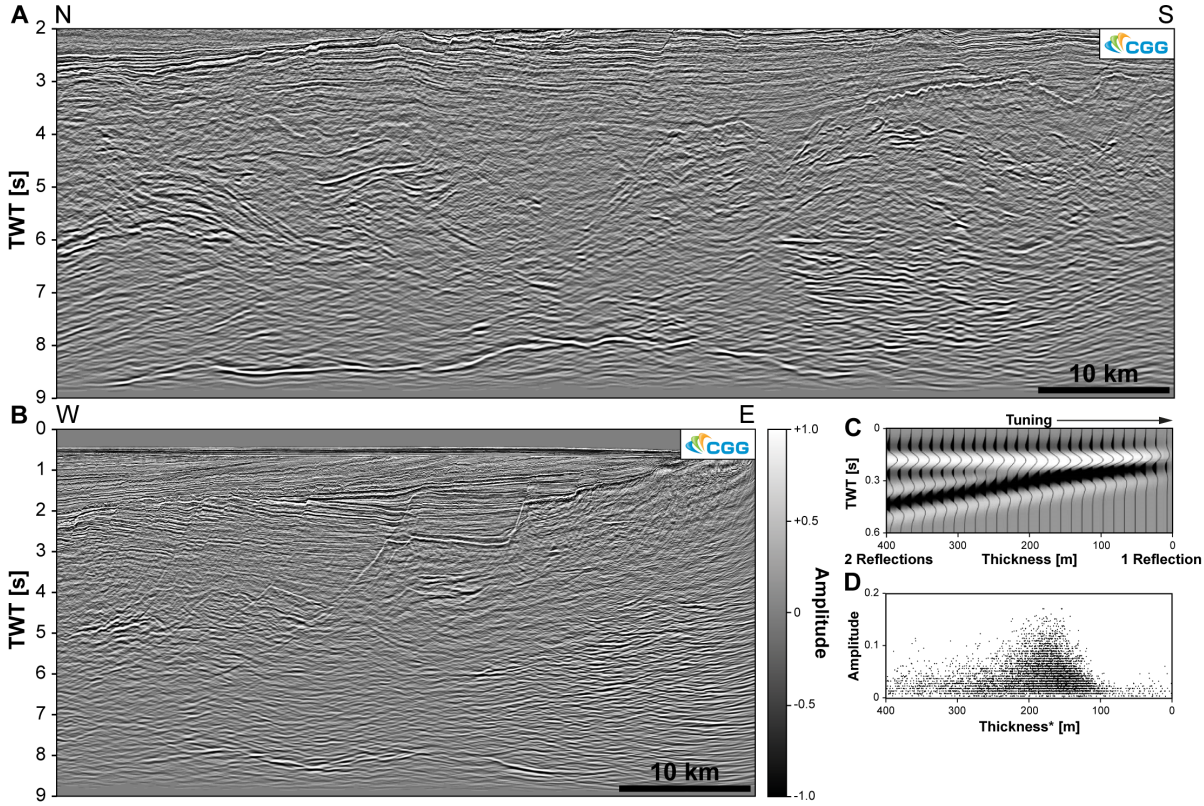

Supp. Figure 1: Uninterpreted version of Figure 2.

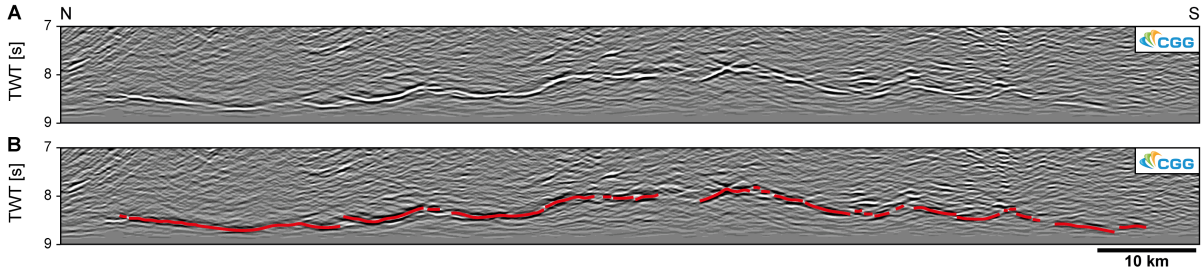

Supp. Figure 2: **A** Uninterpreted and **B** interpreted seismic section equivalent to Figure 3E.